ACS OMEGA

Open Access

http://pubs.acs.org/journal/acsodf

Article

Thermally Stable Al_2O_3/PTFE Composite Separator for High-Safety Lithium-Ion Batteries

Kwang Won Kim, Ji Hyun Lee, Seoyoon Shin, Ilgyu Kim, Tae Gwang Yun, Byungil Hwang, Seon-Jin Choi, Ji-Won Jung, and Ki Ro Yoon*

Cite This: *ACS Omega* 2025, 10, 39669−39679

Read Online

ACCESS | Metrics & More | Article Recommendations | Supporting Information

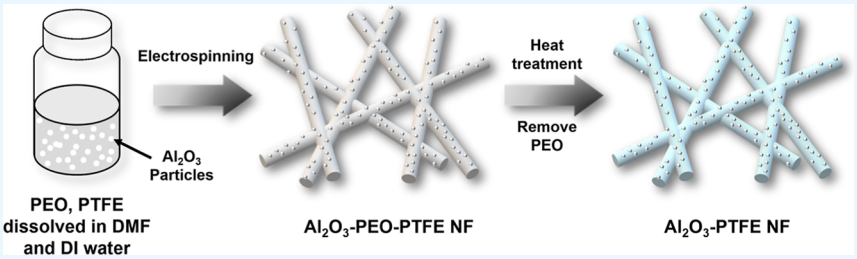

ABSTRACT: In response to the growing demand for carbon neutrality and safer energy storage, advanced separator technology is essential for ensuring the stability of lithium-ion batteries (LIBs). Conventional separators, typically made from polyolefin-based polymers, suffer from low thermal stability and poor wettability, leading to safety and performance concerns. In this study, we fabricated a nonwoven polytetrafluoroethylene (PTFE) nanofiber (NF) separator using emulsion electrospinning incorporating aluminum oxide (Al_2O_3) particles without polymeric binders. The resulting nonwoven PTFE NF separator demonstrated superior porosity, thermal stability, and electrolyte wettability compared to conventional polyolefin-based separators. Its excellent thermal stability and elongation properties make it more durable for practical battery applications. Furthermore, plasma surface modification of the Al_2O_3−PTFE NF enhanced electrolyte wettability, improving ionic conductivity (2.79 mS cm^{-1}) and boosting the overall electrochemical performance of LIB cells. These advancements highlight the PTFE NF separator as a promising candidate for safer, more efficient energy storage components, addressing critical challenges in LIB safety and performance.

1. INTRODUCTION

Due to the growing demand for carbon neutrality and electrification of next-generation energy sources, secondary batteries, such as lithium-ion batteries (LIBs), have emerged as one of the most direct and widely utilized energy storage technologies.[1,2] Their high operating voltage, high energy density, long cycle life, and environmental friendliness make them highly versatile, with applications ranging from portable electronic devices to electric vehicles and energy storage systems.[3−5] Despite their widespread adoption, ensuring safety and reliability, particularly under extreme operating conditions, remains a critical challenge. The thermal stability of battery components, especially the separators, plays a crucial role in preventing thermal runway, which can lead to dangerous incidents such as fires or explosions.[6−8]

The separator, a porous membrane that absorbs the electrolyte and facilitates ion transport while preventing direct contact between the anode and cathode, is a vital component that significantly impacts the stability and performance of LIBs.[9,10] Commonly, LIB separators are made from polyolefin-based materials, such as polyethylene (PE) and polypropylene (PP), due to their excellent chemical stability, high processability and cost-effectiveness.[11−13] However, these materials have relatively low melting points (below 165 °C), which can lead to irreversible thermal shrinkage and melting under high-temperature conditions, causing short circuits and catastrophic battery failure.[14] In addition, their low porosity and nonpolar nature result in poor wettability with organic electrolytes, reducing ionic conductivity and increasing electrochemical impedance in assembled LIBs.[15,16]

To address these challenges, researchers have explored various approaches aimed at improving the thermal stability and wettability of separators. One of the most promising strategies involves using a ceramic-coated separator (CCS), where inorganic particles are applied to the separator using a polymeric binder. Ceramic coatings, due to their inherent surface properties, can enhance separator performance by improving the mechanical strength, thermal resistance, and electrolyte affinity. Among ceramic additives, aluminum oxide

Received: April 4, 2025
Revised: August 15, 2025
Accepted: August 19, 2025
Published: August 25, 2025

(Al_2O_3) is particularly favored as a coating material because of its high surface activity, excellent hydrophilicity derived from the abundant surface hydroxyl (−OH) groups, and superior thermal stability.[17] Deng et al. proposed a CCS incorporating Al_2O_3 and a polymer binder on a PE framework, which exhibited enhanced thermal stability.[18] Similarly, Zhang et al. demonstrated that a separator coated with functionalized Al_2O_3 particles significantly enhanced the electrochemical performance. Notably, the incorporation of amino groups on the Al_2O_3 surface improved electrolyte wettability, resulting in reduced interfacial resistance.[19] Typically, CCSs utilize polyvinylidene fluoride (PVDF) and polyvinylidene fluoride-*co*-hexafluoropropylene (PVDF-HFP) as binders due to their good compatibility with electrolytes, facilitating effective electrolyte filling within the separator.[20,21] However, these binders are prone to swelling and gelation, which can lead to the delamination of the separator.[22] Their relatively low melting points also can raise concerns regarding long-term thermal stability.[23,24] Moreover, conventional CCSs with surface-coated ceramic layers may physically hinder lithium-ion migration across the separator, thereby increasing interfacial resistance and impairing electrochemical performance.[25] Therefore, developing novel polymeric materials with enhanced thermal properties without the need for polymeric binders is essential to overcoming the limitations of traditional polyolefin-based separators.

Among advanced polymer materials, polytetrafluoroethylene (PTFE), commonly known as Teflon, has been extensively used across various industries, including industrial filters,[26] water treatment membranes,[27] functional fabrics,[28] and medical catheters.[29] PTFE is particularly valued for its high melting point (327 °C), nonflammable nature, excellent chemical resistance, and superior electrical insulation properties, making it a promising candidate for use in battery separators.[30,31] However, the exceptional stability of PTFE comes with challenges, particularly its insolubility in almost solvents, resulting in poor processability and hindering control over thickness and porosity.[32] Additionally, the low friction coefficient of PTFE results in poor wettability with liquid electrolytes and difficulties in ceramic coating, posing obstacles to its application as a separator in LIBs.[33]

In this study, we address the limitations of conventional separators and the challenges associated with processing PTFE by developing a novel CCS based on an electrospun PTFE nanofiber (NF) incorporated with Al_2O_3 particles. Traditional electrospinning techniques require homogeneous polymer solutions or melt-processable polymers, which are unsuitable for PTFE due to its high melting point and poor solubility. To overcome these limitations, we adopted an emulsion-based electrospinning approach in which PTFE particles were dispersed within a PEO matrix solution. This strategy enables the direct fabrication of PTFE composite NFs while maintaining structural porosity after thermal removal of PEO components.[34,35] Specifically, insoluble PTFE powders were emulsified in a poly(ethylene oxide) (PEO) solution containing Al_2O_3 particles, followed by electrospinning and heat treatment to produce a nonwoven Al_2O_3-embedded PTFE (Al_2O_3−PTFE) NF network. The resulting NF separator exhibited superior porosity (69%) compared to conventional polyolefin-based separators, which is critical for maintaining the ionic conduction pathway. Furthermore, the inherent thermal stability and elongation properties of the PTFE-based NF make it more robust for practical battery application. Moreover, plasma surface modification of the PTFE NF separator enhances its electrolyte wettability, resulting in a remarkable ionic conductivity (2.79 mS cm^{-1}) and superior electrochemical properties in LIB cells. This study represents a significant advancement in the development of high-performance and thermally stable separators for LIBs. Moreover, our findings open new avenues for the application of PTFE NFs and their potential as a key material for safer and more efficient energy storage systems in the future.

2. EXPERIMENTAL SECTION

2.1. Materials. Poly(ethylene oxide) (PEO, M_w = 900,000 g mol^{-1}), γ-aluminum oxide (γ-Al_2O_3, <50 nm), *N*-methyl-2-pyrrolidone (NMP, ≥99%), and 1 M lithium hexafluorophosphate ($LiPF_6$) in ethylene carbonate/diethyl carbonate (EC/DEC) = 50/50 (v/v) solution were purchased from Sigma-Aldrich Chemistry (USA). *N*,*N*-Dimethylformamide (DMF) was purchased from DAEJUNG Chemicals and Metals (Korea). Polyvinylidene fluoride (PVDF) was purchased from Solef (Belgium). Polytetrafluoroethylene dispersion (PTFE dispersion, Teflon PTFE DISP 30, 60 wt %) was purchased from NARA Cell-TECH (Korea). Commercial polyolefin-based separators, PP (2400), coated PP (3501), and PP/PE/PP trilayer (2320), were purchased from CELGARD (USA). Lithium nickel cobalt manganese oxide (NCM811) was purchased from POSCO FUTURE M (Korea). Li metal (thickness = 0.5 mm) was purchased from Thermo Fisher Scientific (USA). Carbon black (Ketjen black, EC-600JD) was purchased from Nouryon (Netherlands).

2.2. Preparation of Pure PTFE and Al_2O_3−PTFE NF Separators. Due to the insolubility of PTFE polymers in most polar organic solvents commonly used for electrospinning, a modified method was employed to prepare the spinning solution.[34,35] To prepare the PTFE precursor solution, 0.4 g of the copolymer PEO was dissolved in a solvent mixture of 2.5 g of DMF and 5.0 g of deionized (DI) water at room temperature with magnetic stirring. Subsequently, 5.5 g of the PTFE dispersion was added to this mixture to prepare an emulsified solution. To prevent the PTFE particles from agglomerating, the PTFE dispersion was predispersed for about 1 h before mixing. In the case of Al_2O_3−PTFE precursor solution, 0.34 g of Al_2O_3 particles was added during the process of dissolving PEO in the solvent mixture. The prepared solution was loaded into a syringe, and a 21G needle was injected at a flow rate of 1.0 mL h^{-1}. A high DC voltage of 10 kV was applied to the syringe needle containing the solution, and the distance between the tip of the needle and the collector was maintained at 15 cm during the electrospinning. The electrospinning process was conducted at an ambient temperature of 25 °C with a relative humidity of 35%. Following the electrospinning process, the PEO was removed by heat treatment in an air atmosphere at 350 °C for 10 min at a heating rate of 10 °C min^{-1}.

2.3. Material Characterization. The morphology and composition of prepared samples were characterized by using scanning electron microscopy (SEM, SU8000, Hitachi, Japan), energy-dispersive X-ray spectroscopy (EDS, VEGA II SBH, TESCAN, Czech), and Fourier-transform infrared spectroscopy (FT-IR, Spectrum Two, PerkinElmer Inc., USA). X-ray diffraction (XRD, D/MAX-2500/PC, Rigaku, Japan) analysis was conducted using Cu Kα (wavelength = 1.54 Å) radiation in the 10°−80° range. FT-IR spectra were measured in the wavenumber range 400−4000 cm^{-1}. Thermogravimetric

https://doi.org/10.1021/acsomega.5c03086
ACS Omega 2025, 10, 39669−39679

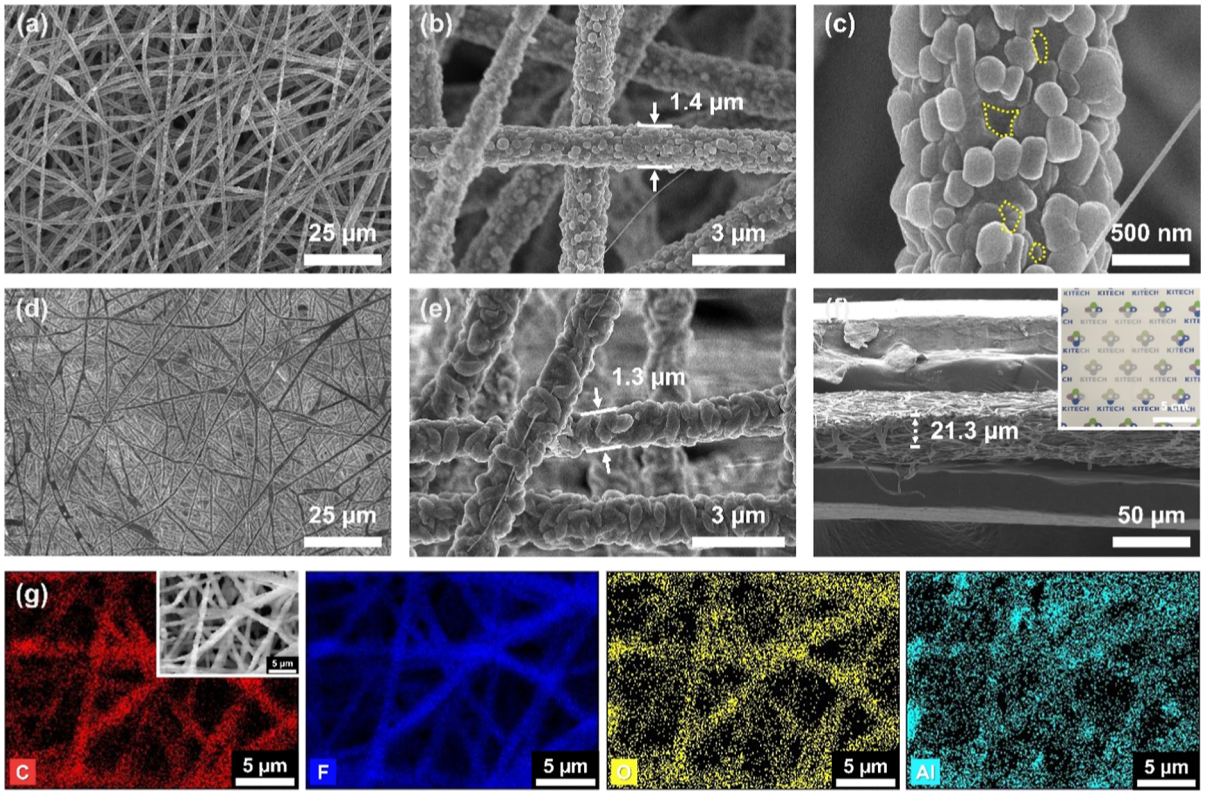

Figure 1. (a) Low-, (b) medium-, and (c) high-magnification SEM images of the Al_2O_3−PEO−PTFE NF. (d) Low- and (e) medium-magnification SEM images of the Al_2O_3−PTFE NF. (f) Cross-sectional SEM and digital photograph image (inset) of the Al_2O_3−PTFE NF. (g) EDS elemental mapping of the Al_2O_3−PTFE NF.

analysis (TGA, Q500, TA Instruments, USA) measurement was performed to evaluate the thermal stability of the separators in the temperature range of 30−800 °C at a heating rate of 20 °C min^{-1} and a flow rate of 50 mL min^{-1} under a nitrogen atmosphere. The thermal shrinkage of separators was assessed by measuring the change in dimension (based on area, 2 × 2 cm^2) following exposure to heat treatment at different temperatures for 1 h, and the value of shrinkage can be calculated using the following eq 1:[36]

$$\text{Shrinkage}\ (\%) = \frac{(S_0 - S)}{S_0} \times 100\% \quad (1)$$

where S_0 and S are the areas of the separator before and after thermal treatment, respectively. Thermographic images of the separators (2 × 4 cm^2) were captured using a thermal imaging camera (E96 24°, FLIR, USA) while the separators were heated on a hot plate maintained at 130 °C. Images were taken at fixed time intervals of 0, 30, 60, 120, and 180 s after sample placement.

The mechanical properties of separators were assessed using a universal testing system (3300, INSTRON, USA). Separators, measuring 1 × 3 cm^2 in size, were cut and positioned at the center of the upper and lower fixtures of the Instron equipment. Tensile testing was conducted at a rate of 10 mm min^{-1} to obtain the stress−strain curves. The porosities of the prepared separators were determined using mercury porosimetry (AutoPore IV 9500, Micromeritics Instrument, USA). The mean pore diameter was measured using a capillary flow porometer (CFP-1500AEX, Porous Materials Inc., USA). The wettability of separators was determined using a contact angle meter (DSA100, KRÜSS, Germany).

The ionic conductivity (σ) of separators was determined by using AC impedance spectroscopy (Zive SM6, WonATech, Korea). Each separator was fully immersed in a liquid electrolyte and then assembled into stainless steel (SS)/separator/SS cells by sandwiching the separator between two SS electrodes. The cell was tested within a frequency range of 0.001 to 10^6 Hz with an amplitude of 5 mV. The ionic conductivity was calculated using the following eq 2[10]

$$\sigma = \frac{d}{R_b \times S} \quad (2)$$

where d is the thickness of the separator, R_b is the bulk resistance between the separator and the electrolyte, and S is the area of the separator.

2.4. Fabrication and Performance Evaluation of LIB Cells. The cathode was prepared by coating a mixture of NCM811 powders, carbon black, and PVDF (8:1:1, w/w/w) onto Al foil, followed by predrying at 100 °C for 40 min. Subsequently, the electrode was calendared and then thoroughly dried at 120 °C in a vacuum oven. The Al_2O_3−PTFE NF separator underwent additional surface modification using a plasma cleaner and etcher (Tergeo, PIE Scientific, USA). The plasma chamber was first evacuated and purged with nitrogen gas to remove residual gases. Ar gas was then introduced at a flow rate of 10 sccm, and plasma treatment was conducted for 1 min at a power of 20 W.

For electrochemical testing, 2032-type coin cells (NCM811/separator/Li metal) were assembled inside an Ar glovebox, using 1 M $LiPF_6$ in (EC/DEC) as the electrolyte. After being assembled, the LIB cells were aged for 12 h before evaluating. To evaluate the electrochemical performances of LIB cells,

https://doi.org/10.1021/acsomega.5c03086
ACS Omega 2025, 10, 39669−39679

Table 1. Microstructures and Various Properties of Pure PTFE, Al_2O_3−PTFE NFs, and Commercial Separators (PP, Coated PP, and PP/PE/PP Trilayer)

Sample	PP	Coated PP	PP/PE/PP	PTFE	Al_2O_3-PTFE
SEM image	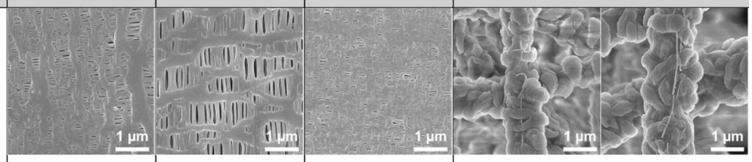				
Thickness (μm)	25	25	20	20	20
Pore size (μm)	0.04	0.06	0.03	2.99	3.11
Porosity (%)	46	47	45	61	69
Thermal shrinkage @ 150 °C (%)	45	25	62	0	0
Tensile strength (MPa)	158	190	202	4.0	5.6
Strain (%)	26	25	17	136	115
Electrolyte contact angle (°)	58	44	47	126	23

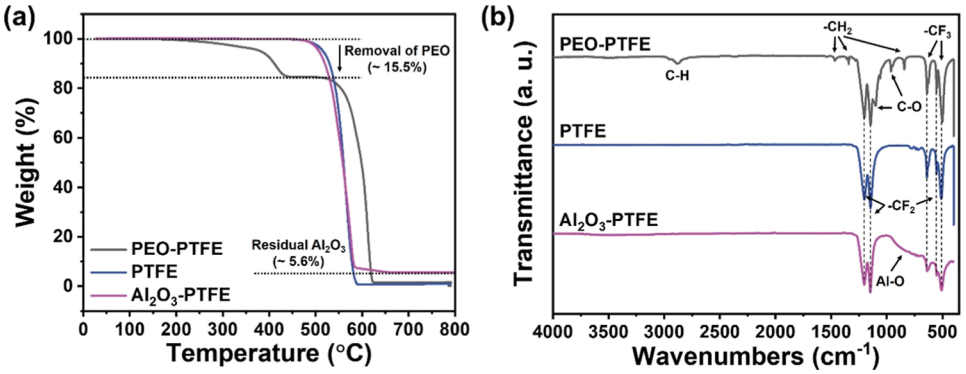

Figure 2. (a) TGA and (b) FT-IR curves of as-spun PEO−PTFE, PTFE, and Al_2O_3−PTFE NFs.

charge−discharge curves were obtained using a multichannel battery-testing system (WBCS3000L, Won-ATech, Korea) under ambient conditions. The charge−discharge curves were tested at 0.5 C within the 2.8−4.2 V voltage range. The rate performance was evaluated at current densities of 0.2, 0.5, 1, and 2 C. Cyclic voltammetry (CV) was performed using an electrochemical workstation (Zive SM6, WonAtech, Korea) with a scan rate of 0.1 mV s^{-1} in the potential range of 2.8−4.2 V.

3. RESULTS AND DISCUSSION

Figure 1a,b presents SEM images of as-spun Al_2O_3−PEO−PTFE NFs (top-view) fabricated via a combination of the emulsification and electrospinning processes. The randomly networked nonwoven NF structure was successfully formed after electrospinning of the Al_2O_3 composite polymer solution. The as-spun composite NFs have an average diameter of approximately 1.4 μm, with PTFE powders embedded within each NF (Figure 1b). A more magnified image reveals the presence of smaller particles, which are attributed to the Al_2O_3 particles (measuring less than 50 nm in size) (Figure 1c). Figure 1d shows that the overall NF nonwoven structure is preserved after heat treatment at 350 °C for 10 min, with noticeable grain growth in PTFE particles (Figure 1e). The overall NF diameter slightly decreased to 1.3 μm, suggesting the pyrolysis of some organic or precursor components during heat treatment. The mean pore diameter and porosity of the Al_2O_3−PTFE NF were analyzed using a capillary flow porometer and mercury porosimetry. The Al_2O_3−PTFE NF exhibited a significantly larger pore size, with a mean pore diameter of 3.11 μm, and higher porosity (69%) than commercially available separators (Table 1). These characteristics allow the separator to accommodate a greater amount of electrolyte through its larger pores when applied to LIBs, thereby facilitating more efficient ion conduction. Figure 1f shows the cross-sectional SEM image and a digital photograph (inset) of the fabricated Al_2O_3−PTFE NF, which has a thickness of 21.3 μm, thin enough to reveal the "KITECH" logo behind it. The thickness of the NFs can be easily adjusted by controlling the electrospinning time, as demonstrated in Figure S1.

Figures S2 and 1g display the EDS spectra and corresponding elemental mapping images of the nonwoven Al_2O_3−PTFE NF. The atomic ratios of carbon, fluorine, oxygen, and aluminum in the Al_2O_3−PTFE NF were measured to be 18.88%, 60.79%, 6.95%, and 13.39%, respectively, indicating the presence of the fluorocarbon-based PTFE polymer and Al_2O_3 components. The EDS mapping images clearly show that aluminum atoms are homogeneously distributed throughout the NFs, supporting that Al_2O_3 particles are embedded within the NF backbone without

https://doi.org/10.1021/acsomega.5c03086
ACS Omega 2025, 10, 39669−39679

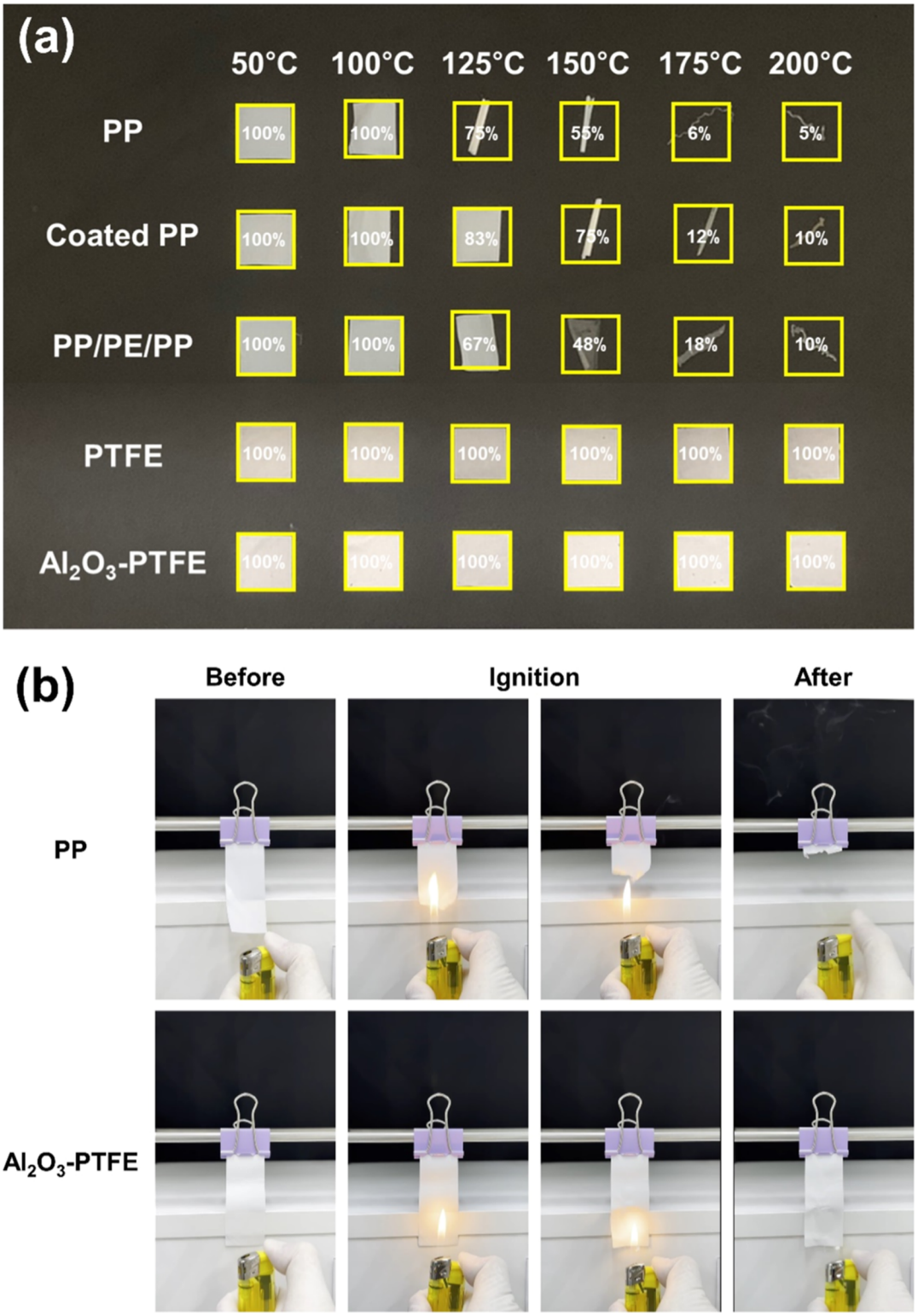

Figure 3. (a) Digital photograph image of the thermal dimensional variation for commercial PP, coated PP, and PP/PE/PP trilayer separators and PTFE and Al_2O_3−PTFE NFs and (b) combustion test of the commercial PP separator and Al_2O_3−PTFE NF.

forming separate phases, as observed in the as-spun sample (Figure 1g). In contrast, the pure PTFE NF, used as a control sample in this study, contained only carbon and fluorine at 17.28% and 82.72%, respectively, with no detectable oxygen or aluminum (Figure S3). These results confirm the successful incorporation of Al_2O_3 particles into the PTFE NFs.

XRD analysis was employed to investigate the presence of Al_2O_3 particles and any phase transformations following high-temperature heat treatment (Figure S4). The peaks at 32.5°, 37.1°, 39.4°, 45.8°, 61.0°, and 67.1° correspond to the (220), (311), (222), (400), (511), and (440) reflection planes of γ-Al_2O_3, respectively.[37,38] Notably, no shift in these peak positions was observed after 350 °C heat treatment, confirming

https://doi.org/10.1021/acsomega.5c03086
ACS Omega 2025, 10, 39669−39679

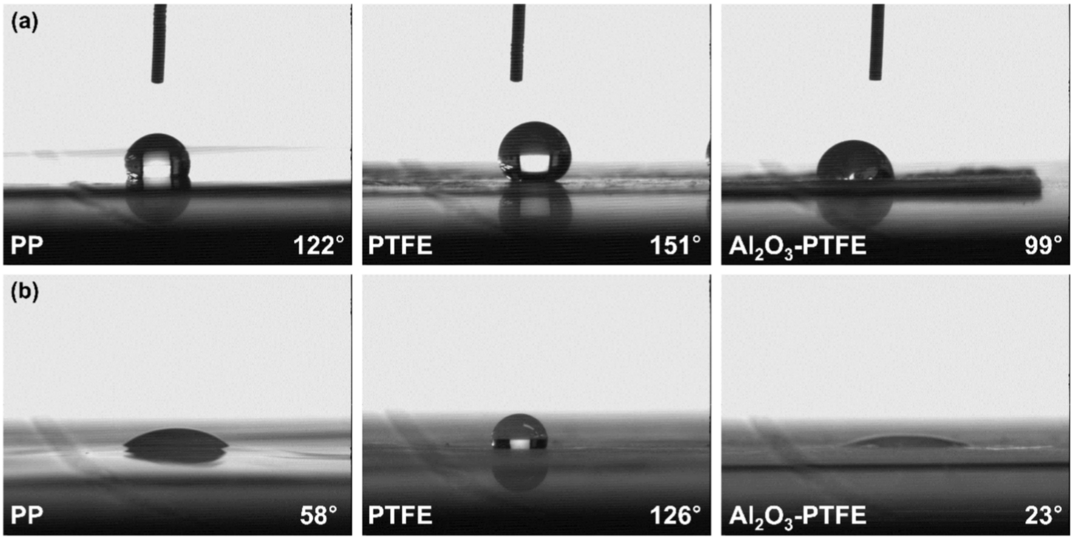

Figure 4. Contact angle measurements of the PP separator, PTFE, and Al_2O_3−PTFE NFs using (a) DI water and (b) 1 M $LiPF_6$ in EC/DEC.

the phase stability of Al_2O_3 within this temperature range. As shown in Figure S5, the PTFE domain exhibits a strong diffraction peak at 18°, corresponding to the (100) plane, along with weaker peaks at 31.4°, 36.9°, and 41.1°, corresponding to the (110), (200), and (108) planes, respectively.[39,40] Following heat treatment, the disappearance of PEO-related peaks at 19.2° (120) and 23.3° (112) in PEO−PTFE and Al_2O_3−PEO−PTFE NFs indicates complete removal of the PEO matrix.[41,42] Nevertheless, the persistence of characteristic γ-Al_2O_3 reflections at 45.8° and 67.1°, corresponding to the (400) and (440) planes in the Al_2O_3−PEO−PTFE and Al_2O_3−PTFE NFs, confirms the presence of Al_2O_3 within the NF matrix.

Figure 2a shows the TGA curves for the as-spun PEO−PTFE, PTFE, and Al_2O_3−PTFE NFs. The as-spun PEO−PTFE NF exhibited a weight loss of approximately 15.5% in the temperature range of 200 to 440 °C, attributed to the thermal decomposition of the PEO component. In contrast, both PTFE and Al_2O_3−PTFE NFs exhibited no significant weight loss up to around 470 °C, indicating that the PEO was completely removed after heat treatment at 350 °C. This suggests that the high thermal stability of these samples is primarily due to the PTFE and Al_2O_3 components. At higher temperatures, thermal decomposition of the PTFE matrix occurred. Unlike the PEO−PTFE and PTFE NFs, the Al_2O_3−PTFE NF retained approximately 5.6% of its weight beyond 600 °C, which can be attributed to the presence of residual Al_2O_3 particles.

Figure 2b shows the FT-IR results for the as-spun PEO−PTFE, PTFE, and Al_2O_3−PTFE NFs. In the PEO−PTFE NF spectrum, distinct PEO-related bands are observed at 2880 cm^{-1}, corresponding to C−H bonds, as well as at 1,467, 1,342, and 842 cm^{-1}, associated with $-CH_2$ bonds, and at 1100 and 962 cm^{-1}, corresponding to C−O bonds.[34,35,43] Notably, these bands are absent in the spectra of both PTFE and Al_2O_3−PTFE NFs, indicating removal of the PEO matrix following heat treatment. In the spectrum of the Al_2O_3−PTFE NFs, broad bands are observed in the range of 400 to 1000 cm^{-1}, attributed to the characteristic absorption of Al_2O_3.[44]

As previously mentioned, the thermal stability of the separator is one of the most critical factors in determining the overall safety of the LIBs. Figure 3a shows the dimensional stability of the manufactured PTFE NF, Al_2O_3−PTFE NF, and commercial polyolefin-based separators (PP, coated PP, PP/PE/PP trilayer) concerning the various temperatures. The PP, coated PP, and PP/PE/PP trilayer separators experienced thermal shrinkage to 55, 75, and 48% of their original size at 150 °C, respectively, and shrank further to 5, 10, and 10% at 200 °C, respectively, losing most of their original form. In contrast, the PTFE and Al_2O_3−PTFE separators maintained their shape without noticeable shrinkage up to 200 °C. To further evaluate the thermoregulating behavior of the separators, temperature variations over time were monitored by using a thermal imaging camera while the samples were placed on a hot plate (Figure S6). When exposed to a surface temperature of 130 °C, the commercial PP separator exhibited a slightly faster increase in surface temperature, reaching approximately 118 °C within 180 s. In contrast, the Al_2O_3−PTFE NF reached about 104 °C under identical conditions. Although both separators showed comparable initial heating rates, PP maintained a modestly higher temperature profile throughout the test, resulting in a final temperature difference of around 14 °C. This moderate yet consistent temperature difference reflects the Al_2O_3−PTFE NF's fibrous porous architecture and the presence of Al_2O_3 nanoparticles, which together help suppress heat transfer through the separator. This advantage arises from its unique fibrous and highly porous structure. PTFE itself has a relatively low thermal conductivity (~0.25 W m^{-1} K^{-1}),[45] and electrospinning reduces the fiber volume fraction while introducing large fiber-to-fiber contact resistance, thereby disrupting thermal conduction pathways.[46,47] In addition, the high porosity (69%) traps air with an even lower thermal conductivity (~0.026 W m^{-1} K^{-1}),[48] and the Al_2O_3 nanoparticles dispersed on the fibers introduce additional interfacial thermal resistance, further suppressing heat transfer through the separator.[49] The PP separator possesses a relatively low porosity (46%) and a highly interconnected structure, which facilitate direct and rapid thermal conduction from the hot surface throughout the material (Figure S7). During battery operation, localized overheating (hotspots) frequently occurs during charging and discharging processes, which can induce shrinkage and thermal decomposition of conventional separators. The thermal insulation properties of the Al_2O_3−PTFE NF separator

https://doi.org/10.1021/acsomega.5c03086
ACS Omega 2025, 10, 39669−39679

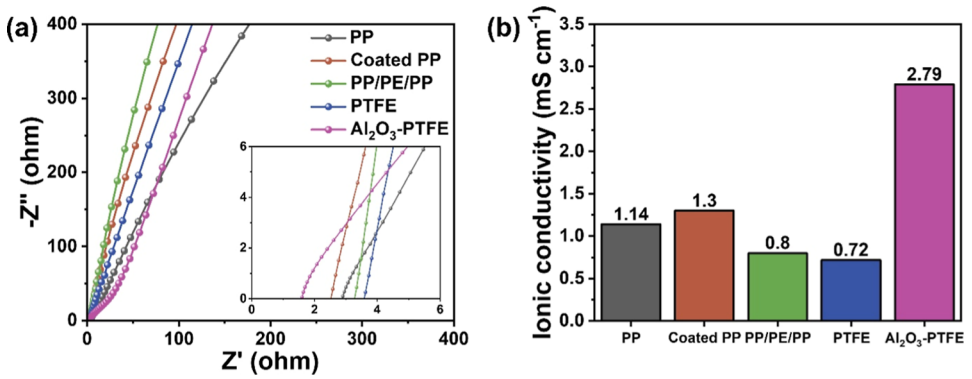

Figure 5. (a) Nyquist plots and (b) ionic conductivities of commercial PP, coated PP, and PP/PE/PP trilayer separators and pure PTFE and Al_2O_3−PTFE NFs.

effectively suppress heat conduction, mitigating hotspot formation and enhancing cell safety.[50] Furthermore, improved thermal resistance enables the separator to maintain dimensional stability and a porous structure at high temperatures without pore collapse or shrinkage. This ensures stable electrochemical performance and helps prevent catastrophic failures, such as thermal runaway.

The flame retardancy of the separator is another crucial factor in ensuring the safety of the LIBs. To assess this, a combustion test was conducted on both commercial PP and Al_2O_3−PTFE NF separators. As shown in Figure 3b, the Al_2O_3−PTFE NF demonstrated strong resistance to combustion due to its inherent flame-retardant properties, while the commercial PP separator was completely consumed immediately upon exposure to fire. The excellent flame retardancy of the Al_2O_3−PTFE NF is expected to significantly reduce the risk of thermal runaway or fire when used as an LIB separator.

The wettability of the separator is a crucial factor that directly influences the Li^+ ion transport through the electrolyte, thereby affecting the overall performance of the LIB cells. The effect of Al_2O_3 incorporation on the wettability was characterized by measuring the contact angles using both DI water and 1 M $LiPF_6$ in EC/DEC, an organic electrolyte commonly used in LIBs. As shown in Figure 4a, the PP separator and the pure PTFE NF separator exhibited water contact angles of 122° and 151°, respectively, indicating their intrinsic hydrophobicity. The extremely high hydrophobicity and poor wettability of the PTFE NF are due to the highly stable fluorocarbon structure of the PTFE molecules. However, upon incorporation of Al_2O_3, the contact angle significantly decreased to 99°, indicating a notable enhancement in hydrophilicity. A similar trend was observed when measured with the organic electrolyte (Figure 4b).[51] While the PTFE NF showed a slightly larger contact angle of 126°, the Al_2O_3−PTFE NF demonstrated a drastically reduced contact angle of 23°, confirming the strong affinity of Al_2O_3 toward the polar organic electrolyte.[17] These results clearly indicate that the incorporation of Al_2O_3 improves the surface wettability of the separator, which is beneficial for the electrolyte uptake and ion conduction in LIBs.

Furthermore, a tensile strength test was conducted on the PP, coated PP, and PP/PE/PP trilayer separators and PTFE and Al_2O_3−PTFE NFs to evaluate their suitability as LIB separators. The stress−strain curves of the separators and the corresponding digital photographic images of the tensile strength tests are presented in Figure S8. The commercial separators, PP, coated PP, and PP/PE/PP trilayer, exhibited relatively high tensile stress values of 158, 111, and 202 MPa, respectively, but had extremely low strain values of only around 20%. In contrast, the PTFE-based separators exhibited lower tensile stress values below 10 MPa due to their NF structure. Nevertheless, the PTFE and Al_2O_3−PTFE NFs demonstrated impressive strain values of 136% and 115%, respectively. The incorporation of ceramic alumina particles enhanced the tensile stress of the Al_2O_3−PTFE NF (5.6 MPa) compared to that of the pure PTFE NF (4.0 MPa). Although the strain slightly decreased, it still showed a significant improvement over the commercial separators. This indicates that the Al_2O_3−PTFE NF can effectively prevent short circuits by accommodating the deformation of the battery under external impacts. The various properties of the pure PTFE NF and Al_2O_3−PTFE NF, compared with the commercial separators (PP, coated PP, and PP/PE/PP trilayer), are summarized in Table 1.

The performance of LIBs is significantly influenced by the movement of Li^+ through the separators, which is directly related to the separator's ionic conductivity. The Nyquist plots obtained from electrochemical impedance spectroscopy (EIS) of the separators containing electrolytes, assembled with stainless steel (SS)/separator/SS cells, are displayed in Figure 5a. The bulk resistance of the separators was determined from the *x*-axis intercept, and the calculated ionic conductivities of the separators are shown in Figure 5b. The bulk resistances of the commercial separators (PP, coated PP, and PP/PE/PP trilayer) were 2.79, 2.45, and 3.21 Ω, respectively. These high resistance values can be attributed to the small pore size, low porosity (Table 1), and electrolyte wettability of the separator. Although the PTFE NF separator possesses high porosity and a fibrous structure with a large surface area, its inherently nonpolar nature makes it difficult to form effective contact with the electrolyte,[52] resulting in a high electrical resistance value of 3.52 Ω. The ionic conductivities of PP, coated PP, PP/PE/PP trilayer separators and the PTFE NF, calculated from their respective resistance values, were 1.14, 1.30, 0.79, and 0.72 mS cm^{-1}, respectively (Figure 5b). In contrast, the Al_2O_3−PTFE NF exhibited a significantly lower bulk resistance of 1.59 Ω, resulting in an impressive ionic conductivity of 2.78 mS cm^{-1}. This value is among the highest reported to date for LIB separators (Table S1). These improvements result from the effects of several factors. First, the large pore size and high porosity of the NF provide a basis for accommodating a larger amount of electrolyte when the separator is immersed in liquid

https://doi.org/10.1021/acsomega.5c03086
ACS Omega 2025, 10, 39669−39679

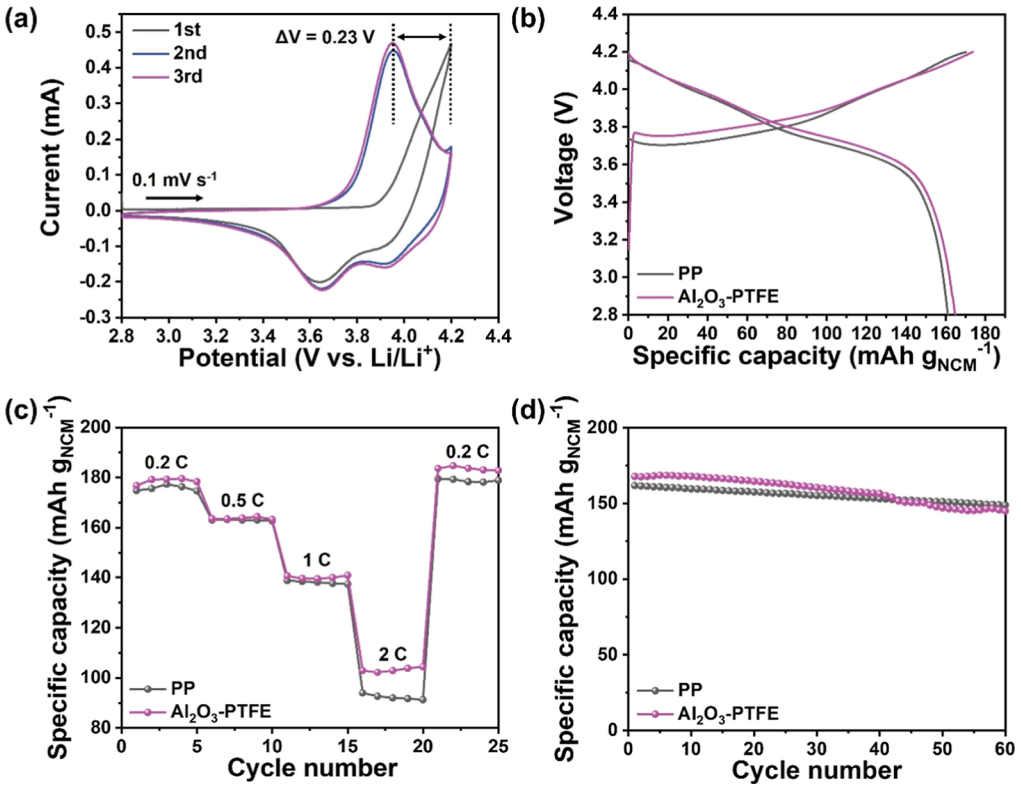

Figure 6. Electrochemical behavior of NCM811/Li half cells. (a) CV curves of three cycles at a scan rate of 0.1 mV s^{-1} of the Al_2O_3−PTFE NF. (b) First charge−discharge capacity profiles of the PP separator and Al_2O_3−PTFE NF at 0.5 C. (c) Rate capability at 0.2, 0.5, 1, and 2 C. (d) Cycling performance of the PP separator and Al_2O_3−PTFE NF in the voltage range of 2.8−4.2 V.

electrolyte. Second, the Al_2O_3 particles embedded in the PTFE NF and plasma surface modification enhance the hydrophilicity of the PTFE-based NF and can provide excellent compatibility with polar electrolytes.[20]

To evaluate the feasibility of the Al_2O_3−PTFE NF as a separator for LIBs, 2032-type coin cells were assembled by using a Li metal anode and NCM811 cathode. CV was conducted for three cycles between 2.8 and 4.2 V at a scan rate of 0.1 mV s^{-1} (Figures 6a and S9). As shown in Figure S9, the cell using a PP separator exhibited well-defined oxidation and reduction peaks within this voltage window, corresponding to the extraction and insertion of Li^+ ions and the Ni^{2+}/Ni^{4+} redox reactions of the NCM811 cathode material.[53,54] Similarly, the cell incorporating the Al_2O_3−PTFE NF separator (Figure 6a) displayed comparable redox peaks with no additional signals that could indicate side reactions. This confirms that the Al_2O_3−PTFE NF does not interfere with the electrochemical process of the cell. Furthermore, the potential difference between the anodic peaks of the first and third cycles (ΔV), commonly used as an indicator of electrode polarization,[55] was evaluated. The ΔV for the Al_2O_3−PTFE NF was measured to be 0.23 V, which is lower than the 0.28 V observed with the PP separator. This suggests reduced polarization and improved electrochemical kinetics and reversibility of the cell.

The electrochemical performance of the assembled cells was assessed through charge−discharge measurements. As shown in Figure 6b, the cell employing the PP separator delivered charge and discharge capacities of 170 and 161 mAh g^{-1}, respectively. In comparison, the cell utilizing the Al_2O_3−PTFE NF separator achieved similar charge and discharge capacities of 173 and 164 mAh g^{-1}, respectively. For all separators, the specific discharge capacity decreased with increasing discharge current density (Figure 6c). However, the cell employing the Al_2O_3−PTFE NF exhibited discharge capacities of 178, 164, 140, and 103 mAh g^{-1} at 0.2, 0.5, 1, and 2 C, respectively, which are slightly higher than those of the cell with the PP separator (175, 163, 138, and 92 mAh g^{-1}, respectively). This consistently enhanced performance across varying current densities demonstrates the superior electrochemical kinetics enabled by the Al_2O_3−PTFE NF. The improved rate capability is attributed to the outstanding ionic conductivity of the separator, which ensures stable operation under high-rate conditions. Furthermore, both the PP separator and Al_2O_3−PTFE NF exhibited stable capacity recovery when the current density was switched from 2 to 0.2 C, confirming their reversible electrochemical behavior. As shown in Figure 6d, the cycling performance of the assembled cells was evaluated over 60 cycles at a constant charge current density of 0.5 C within a voltage range of 2.8−4.2 V. The discharge capacity of the cell exhibited a gradual decline with cycling, which can be attributed to the progressive increase in internal resistance caused by physical changes in the active materials and interfacial degradation.[56] The cell with the PP separator retained approximately 90.7% of its initial discharge capacity, while the Al_2O_3−PTFE NF retained 87.4%, demonstrating cycling stability comparable to that of the commercial separator.

4. CONCLUSIONS

Through the emulsion electrospinning of Al_2O_3 and PTFE-added PEO solution, we successfully developed a nonwoven Al_2O_3-PTFE NF separator without the need for a polymeric

https://doi.org/10.1021/acsomega.5c03086
ACS Omega 2025, 10, 39669−39679

binder. The inherent structural properties of PTFE provided the fabricated nonwoven separator with excellent thermal stability and elongation properties. The plasma surface modification of the PTFE NF separator further enhanced the electrolyte wettability of the Al_2O_3−PTFE NF separator. In addition, its high porosity (69%), combined with the excellent compatibility of Al_2O_3 with the polar solvent, resulted in a remarkable ionic conductivity (2.79 mS cm^{-1}). These advantageous features contributed significantly to the overall electrochemical performance of the fabricated LIB cell. We believe that this efficient fabrication method for the Al_2O_3−PTFE NF separator paves the way for the production of safer, higher-performing LIBs.

■ ASSOCIATED CONTENT

Supporting Information

The Supporting Information is available free of charge at https://pubs.acs.org/doi/10.1021/acsomega.5c03086.

Cross-sectional SEM images of Al_2O_3−PTFE NFs with various thicknesses; EDS spectra of the Al_2O_3−PTFE NF; EDS spectra and elemental mapping images of the pure PTFE NF; XRD patterns of the Al_2O_3 particles before and after heat treatment; XRD patterns of the PEO−PTFE, PTFE, Al_2O_3−PEO−PTFE, and Al_2O_3−PTFE NFs; Thermal management test of the PP separator and Al_2O_3−PTFE NFs; Cross-sectional SEM image of the PP separator; Stress−strain curves of PP, coated PP, and PP/PE/PP trilayer separators and PTFE and Al_2O_3−PTFE NFs, and corresponding digital photographic images before fracture; CV curves of three cycles at a scan rate of 0.1 mV s^{-1} of the PP separator; Comparison of ionic conductivity values of previously reported separators (PDF)

■ AUTHOR INFORMATION

Corresponding Author

Ki Ro Yoon − *Textile Innovation R&D Department, Korea Institute of Industrial Technology, Ansan-si, Gyeonggi-do 15588, Republic of Korea;* Present Address: Department of Materials Science and Engineering, Konkuk University, 120, Neungdong-ro, Gwangjin-gu, Seoul 05029, Republic of Korea; orcid.org/0000-0003-3532-7911; Email: kryoon@konkuk.ac.kr

Authors

Kwang Won Kim − *Textile Innovation R&D Department, Korea Institute of Industrial Technology, Ansan-si, Gyeonggi-do 15588, Republic of Korea; Division of Materials Science and Engineering, Hanyang University, Seoul 04763, Republic of Korea*

Ji Hyun Lee − *Textile Innovation R&D Department, Korea Institute of Industrial Technology, Ansan-si, Gyeonggi-do 15588, Republic of Korea; Division of Materials Science and Engineering, Hanyang University, Seoul 04763, Republic of Korea*

Seoyoon Shin − *Hydrogen Digital Convergence Center, Korea Institute of Ceramic Engineering and Technology, Jinju 52851, Republic of Korea;* orcid.org/0000-0001-6544-8824

Ilgyu Kim − *Department of Materials Science and Engineering, KonKuk University, Seoul 05029, Republic of Korea*

Tae Gwang Yun − *Department of Molecular Science and Technology, Ajou University, Suwon-si, Gyeonggi-do 16499, Republic of Korea*

Byungil Hwang − *School of Integrative Engineering, Chung-Ang University, Seoul 06974, Republic of Korea;* orcid.org/0000-0001-9270-9014

Seon-Jin Choi − *Division of Materials Science and Engineering, Hanyang University, Seoul 04763, Republic of Korea;* orcid.org/0000-0001-8567-0668

Ji-Won Jung − *Department of Materials Science and Engineering, KonKuk University, Seoul 05029, Republic of Korea; Advanced Materials Program, Department of Materials Science and Engineering, Konkuk University, Seoul 05029, Republic of Korea*

Complete contact information is available at: https://pubs.acs.org/10.1021/acsomega.5c03086

Notes

The authors declare no competing financial interest.

■ ACKNOWLEDGMENTS

This research was supported by National R&D Program through the National Research Foundation of Korea (NRF) funded by Ministry of Science and ICT (MSIT) (RS-2022-NR067638) and GRDC (Global Research Development Center) Cooperative Hub Program through the National Research Foundation of Korea (NRF) funded by MSIT (RS-2023-00257595).

■ REFERENCES

(1) Lin, J.; Zhang, X.; Fan, E.; Chen, R.; Wu, F.; Li, L. Carbon neutrality strategies for sustainable batteries: from structure, recycling, and properties to applications. *Energy Environ. Sci.* **2023**, *16* (3), 745−791.

(2) Qiao, D.; Ma, Y.; Bao, Y.; Hong, Y.; Dai, T.; Narenmandula; Dai, T. Exploring the potential impact of electric passenger vehicle battery recycling on China's cobalt supply and demand under the goals of carbon peaking and carbon neutrality during 2010−2060. *J. Clean. Prod.* **2024**, *444*, 141139.

(3) Min, X.; Xu, G.; Xie, B.; Guan, P.; Sun, M.; Cui, G. Challenges of prelithiation strategies for next generation high energy lithium-ion batteries. *Energy Storage Mater.* **2022**, *47*, 297−318.

(4) Yu, B.; Chen, X.; Jin, X.; Zhang, X.; Chen, L. Heat-Resistant Lithium-Ion-Battery Separator Using Synchronous Thermal Stabilization/Imidization. *ACS Appl. Polym. Mater.* **2024**, *6* (5), 2464−2473.

(5) Liu, S.; Fan, B.; Shi, Z.; Wan, R.; Sheng, X.; Li, X.; Zhu, C.; Chen, M.; Xue, Z.; Ding, Y.; et al. High-Safety Lithium-Ion Battery Separator with Adjustable Temperature Function Inspired by the Sugar Gourd Structure. *ACS Appl. Mater. Interfaces* **2024**, *16*, 30284−30295.

(6) Gong, S.; Jeon, H.; Lee, H.; Ryou, M.-H.; Lee, Y. M. Effects of an integrated separator/electrode assembly on enhanced thermal stability and rate capability of lithium-ion batteries. *ACS Appl. Mater. Interfaces* **2017**, *9* (21), 17814−17821.

(7) Song, Y.; Wang, L.; Cui, H.; Liang, H.; Hu, Q.; Ren, D.; Yang, Y.; Zhang, H.; Xu, H.; He, X. Boosting Battery Safety by Mitigating Thermal-Induced Crosstalk with a Bi-Continuous Separator. *Adv. Energy Mater.* **2022**, *12* (44), 2201964.

(8) Hu, X.; Gao, F.; Xiao, Y.; Wang, D.; Gao, Z.; Huang, Z.; Ren, S.; Jiang, N.; Wu, S. Advancements in the safety of Lithium-Ion Battery: The trigger, consequence and mitigation method of thermal runaway. *J. Chem. Eng.* **2024**, *481*, 148450.

(9) Waqas, M.; Ali, S.; Feng, C.; Chen, D.; Han, J.; He, W. Recent development in separators for high-temperature lithium-ion batteries. *Small* **2019**, *15* (33), 1901689.

(10) Jiang, F.; Yin, L.; Yu, Q.; Zhong, C.; Zhang, J. Bacterial cellulose nanofibrous membrane as thermal stable separator for lithium-ion batteries. *J. Power Sources* **2015**, *279*, 21−27.
(11) Yuan, B.; Feng, Y.; Qiu, X.; He, Y.; Dong, L.; Zhong, S.; Liu, J.; Liang, Y.; Liu, Y.; Xie, H.; et al. A Safe Separator with Heat-Dispersing Channels for High-Rate Lithium-Ion Batteries. *Adv. Funct. Mater.* **2024**, *34* (9), 2308929.
(12) Wang, Y.; Wang, S.; Fang, J.; Ding, L.-X.; Wang, H. A nano-silica modified polyimide nanofiber separator with enhanced thermal and wetting properties for high safety lithium-ion batteries. *J. Membr. Sci.* **2017**, *537*, 248−254.
(13) Sukenik, E. G.; Kasaei, L.; Amatucci, G. G. Engineering high transport plastic separators for next-generation Li-ion batteries. *Ionics* **2023**, *29* (1), 233−257.
(14) Sun, H.; Liu, Z.; Sang, X.; Li, R.; Li, P.; Hu, X. Mechanically Robust and Safe Separators Based on Inorganic Nanofibers for Lithium-Ion Batteries. *ACS Appl. Energy Mater.* **2024**, *7*, 5537−5547.
(15) Wang, Y.; Zhou, M.; Yang, J.; Zhao, L.; Liu, L.; Li, W.; Huang, Y.; Wang, M. Polyhedral Oligomeric Silsesquioxane Modified Polyolefin Separator for Advanced Lithium−Metal Batteries. *ACS Appl. Energy Mater.* **2024**, *7* (15), 6400−6407.
(16) Deng, J.-h.; Cao, D.-q.; Li, L.-j.; Chen, Y.-p.; Zhang, G.-q.; Yang, X.-q. Electrospun nanofiber separator derived from nano-SiO2-modified polyimide with superior mechanical flexibility for high-performance lithium-ion battery. *J. Mater. Sci.* **2021**, *56* (27), 15215−15228.
(17) Liu, H.; Liu, C.; Zhou, Y.; Zhang, Y.; Deng, W.; Zou, G.; Hou, H.; Ji, X. The application of Al2O3 in separators and solid electrolytes of lithium-ion battery: a review. *Energy Storage Mater.* **2024**, *71*, 103575.
(18) Deng, Y.; Song, X.; Ma, Z.; Zhang, X.; Shu, D.; Nan, J. Al2O3/PVdF-HFP-CMC/PE separator prepared using aqueous slurry and post-hot-pressing method for polymer lithium-ion batteries with enhanced safety. *Electrochim. Acta* **2016**, *212*, 416−425.
(19) Zhang, H.; Sheng, L.; Bai, Y.; Song, S.; Liu, G.; Xue, H.; Wang, T.; Huang, X.; He, J. Amino-functionalized Al2O3 particles coating separator with excellent lithium-ion transport properties for high-power density lithium-ion batteries. *Adv. Eng. Mater.* **2020**, *22* (11), 1901545.
(20) Yu, L.; Jin, Y.; Lin, Y. Ceramic coated polypropylene separators for lithium-ion batteries with improved safety: effects of high melting point organic binder. *RSC Adv.* **2016**, *6* (46), 40002−40009.
(21) Lee, H.; Yanilmaz, M.; Toprakci, O.; Fu, K.; Zhang, X. A review of recent developments in membrane separators for rechargeable lithium-ion batteries. *Energy Environ. Sci.* **2014**, *7* (12), 3857−3886.
(22) Shi, C.; Zhang, P.; Chen, L.; Yang, P.; Zhao, J. Effect of a thin ceramic-coating layer on thermal and electrochemical properties of polyethylene separator for lithium-ion batteries. *J. Power Sources* **2014**, *270*, 547−553.
(23) Shi, C.; Dai, J.; Shen, X.; Peng, L.; Li, C.; Wang, X.; Zhang, P.; Zhao, J. A high-temperature stable ceramic-coated separator prepared with polyimide binder/Al2O3 particles for lithium-ion batteries. *J. Membr. Sci.* **2016**, *517*, 91−99.
(24) Lee, S.; Koo, H.; Kang, H. S.; Oh, K.-H.; Nam, K. W. Advances in polymer binder materials for lithium-ion battery electrodes and separators. *Polymer* **2023**, *15* (23), 4477.
(25) Fan, Z.; Chen, X.; Shi, J.; Nie, H.; Zhang, X.; Zhou, X.; Xie, X.; Xue, Z. Functionalized Separators Boosting Electrochemical Performances for Lithium Batteries. *Nano-Micro Lett.* **2025**, *17* (1), 128.
(26) Kim, H. B.; Han, B.; Lee, M.-H. Enhanced filtration characteristics of a PTFE foam-coated filter using PTFE nanofibers. *Mater. Chem. Phys.* **2023**, *305*, 127970.
(27) Qing, W.; Shi, X.; Deng, Y.; Zhang, W.; Wang, J.; Tang, C. Y. Robust superhydrophobic-superoleophilic polytetrafluoroethylene nanofibrous membrane for oil/water separation. *J. Membr. Sci.* **2017**, *540*, 354−361.
(28) Dong, T.; Zhang, Y.; Yu, M.; Zhang, X.; Ma, P. Surface performance of weft-knitted fabric composites reinforced with polytetrafluoroethylene fibers. *J. Appl. Polym. Sci.* **2022**, *139* (13), 51864.
(29) Zhang, S.; Wang, L.; Liang, X.; Vorstius, J.; Keatch, R.; Corner, G.; Nabi, G.; Davidson, F.; Gadd, G. M.; Zhao, Q. Enhanced antibacterial and antiadhesive activities of silver-PTFE nanocomposite coating for urinary catheters. *ACS Biomater. Sci. Eng.* **2019**, *5* (6), 2804−2814.
(30) Feng, S.; Zhong, Z.; Wang, Y.; Xing, W.; Drioli, E. Progress and perspectives in PTFE membrane: Preparation, modification, and applications. *J. Membr. Sci.* **2018**, *549*, 332−349.
(31) Guo, H.; Li, M.; Li, F.; Zhu, Q.; Zhao, Y.; Wang, F.; Qin, Z. Enhanced Wettability of a PTFE Porous Membrane for a High-Temperature Stable Lithium-Ion Battery Separator. *Chem. Eng. Technol.* **2022**, *45* (4), 737−744.
(32) Xu, H.; Jin, W.; Wang, F.; Liu, G.; Li, C.; Wang, J.; Zhu, H.; Guo, Y. Formation and characterization of polytetrafluoroethylene nanofiber membranes for high-efficiency fine particulate filtration. *RSC Adv.* **2019**, *9* (24), 13631−13645.
(33) Sun, X.; Zhang, L.; Yu, C.; Xie, G.; Li, Y.; Wu, X.; Li, X.; Guo, D. Surface modification of polytetrafluoroethylene (PTFE) fibers through methyl methacrylate (MMA) polymerization for self-lubricating composites. *Appl. Surf. Sci.* **2024**, *660*, 159992.
(34) Hwang, C.-K.; Lee, K. A.; Lee, J.; Kim, Y.; Ahn, H.; Hwang, W.; Ju, B.-K.; Kim, J. Y.; Yeo, S. Y.; Choi, J.; et al. Perpendicularly stacked array of PTFE nanofibers as a reinforcement for highly durable composite membrane in proton exchange membrane fuel cells. *Nano Energy* **2022**, *101*, 107581.
(35) Lee, J. H.; Kim, K. W.; Choi, S.-J.; Yoon, K. R. A Study on the Industrial Application of PTFE Fibrous Nonwoven Fabricated by Electrospinning Technique as Dust Filtration Media. *Text. Sci. Eng.* **2023**, *60* (4), 281−291.
(36) Tong, B.; Li, X. Towards separator safety of lithium-ion batteries: a review. *Mater. Chem. Front.* **2024**, *8* (2), 309−340.
(37) Atrak, K.; Ramazani, A.; Taghavi Fardood, S. Green synthesis of amorphous and gamma aluminum oxide nanoparticles by tragacanth gel and comparison of their photocatalytic activity for the degradation of organic dyes. *J. Mater. Sci.: Mater. Electron.* **2018**, *29*, 8347−8353.
(38) Lee, J.; Jeon, H.; Oh, D. G.; Szanyi, J.; Kwak, J. H. Morphology-dependent phase transformation of γ-Al2O3. *Appl. Catal., A* **2015**, *500*, 58−68.
(39) Si, J.; Ma, R.; Wu, Y.; Dong, Y.; Yao, K. Microstructure and magnetic properties of novel powder cores composed of iron-based amorphous alloy and PTFE. *J. Mater. Sci.* **2022**, *57* (17), 8154−8166.
(40) Chingo Aimacana, C. M.; Quinchiguango Perez, D. A.; Rocha Pinto, S.; Debut, A.; Attia, M. F.; Santos-Oliveira, R.; Whitehead, D. C.; Terencio, T.; Alexis, F.; Dahoumane, S. A. Polytetrafluoroethylene-like nanoparticles as a promising contrast agent for dual modal ultrasound and X-ray bioimaging. *ACS Biomater. Sci. Eng.* **2021**, *7* (3), 1181−1191.
(41) Polu, A. R.; Kim, K.; Kareem, A. A.; Kim, D.; Song, S.; Savilov, S. V.; Singh, P. K. Impact of tetracyanoethylene plasticizer on PEO based solid polymer electrolytes for improved ionic conductivity and solid-state lithium-ion battery performance. *J. Power Sources* **2025**, *625*, 235742.
(42) Song, Y.-W.; Park, S.-J.; Heo, K.; Lee, H.; Hwang, D.; Kim, M.-Y.; Kim, J.; Lim, J. Enhancing Electrochemical Performance in PEO/LLZTO Composite Solid Electrolyte via PEG Polymer Integration for Solid-State Batteries. *Energy Technol.* **2023**, *11* (9), 2300334.
(43) Zhao, P.; Soin, N.; Prashanthi, K.; Chen, J.; Dong, S.; Zhou, E.; Zhu, Z.; Narasimulu, A. A.; Montemagno, C. D.; Yu, L.; et al. Emulsion electrospinning of polytetrafluoroethylene (PTFE) nanofibrous membranes for high-performance triboelectric nanogenerators. *ACS Appl. Mater. Interfaces* **2018**, *10* (6), 5880−5891.
(44) Mallakpour, S.; Dinari, M. Enhancement in thermal properties of poly (vinyl alcohol) nanocomposites reinforced with Al2O3 nanoparticles. *J. Reinf. Plast. Compos.* **2013**, *32* (4), 217−224.
(45) Jin, Z.; Chen, X.; Wang, Y.; Wang, D. Thermal conductivity of PTFE composites filled with graphite particles and carbon fibers. *Comput. Mater. Sci.* **2015**, *102*, 45−50.

https://doi.org/10.1021/acsomega.5c03086
ACS Omega 2025, 10, 39669−39679

(46) Zhao, X.; Huang, C.; Liu, Q.; Smalyukh, I. I.; Yang, R. Thermal conductivity model for nanofiber networks. *J. Appl. Phys.* **2018**, *123* (8), 085103.
(47) Zhu, J.; Zhang, Q.; Zhao, Y.; Zhang, R.; Liu, L.; Yu, J. Robust N-doping porous carbon nanofiber membranes with inter-fiber cross-linked structures for supercapacitors. *Carbon* **2023**, *202*, 13−25.
(48) Knapczyk-Korczak, J.; Szewczyk, P. K.; Berniak, K.; Marzec, M. M.; Frąc, M.; Pichór, W.; Stachewicz, U. Flexible and Thermally Insulating Porous Materials Utilizing Hollow Double-Shell Polymer Fibers. *Adv. Sci.* **2024**, *11* (36), 2404154.
(49) Zhuo, T.; Xin, B.; Chen, Z.; Xu, Y.; Zhou, X.; Yu, J. Enhanced thermal insulation properties of PI nanofiber membranes achieved by doping with SiO2 nanoparticles. *Eur. Polym. J.* **2021**, *153*, 110489.
(50) Quan, T.; Xia, Q.; Wei, X.; Zhu, Y. Recent Development of Thermal Insulating Materials for Li-Ion Batteries. *Energies* **2024**, *17* (17), 4412.
(51) Sun, Y.; Radke, C. J.; McCloskey, B. D.; Prausnitz, J. M. Wetting behavior of four polar organic solvents containing one of three lithium salts on a lithium-ion-battery separator. *J. Colloid Interface Sci.* **2018**, *529*, 582−587.
(52) Zhang, X.; Zheng, Y.; Wang, D.; Rahman, Z. U.; Zhou, F. Liquid−solid contact triboelectrification and its use in self-powered nanosensor for detecting organics in water. *Nano Energy* **2016**, *30*, 321−329.
(53) Xia, Y.; Li, Y.; Xiao, Z.; Zhou, X.; Wang, G.; Zhang, J.; Gan, Y.; Huang, H.; Liang, C.; Zhang, W. *β*-Cyclodextrin-modified porous ceramic membrane with enhanced ionic conductivity and thermal stability for lithium-ion batteries. *Ionics* **2020**, *26*, 173−182.
(54) Liu, W.; Gao, F.; Zang, Y.; Qu, J.; Xu, J.; Ji, S.; Huo, Y.; Qiu, J. Boosting cycle stability of NCM811 cathode material via 2D Mg-Al-LDO nanosheet coating for lithium-ion battery. *J. Alloys Compd.* **2021**, *867*, 159079.
(55) Kim, H.; Jeong, M. K.; Kim, H. J.; Kim, Y.; Kang, K.; Oh, J. H. Enhanced Cycling Stability of NCM811 Cathodes at High C-Rates and Voltages via LiMTFSI-Based Polymer Coating. *Small* **2025**, *21*, 2502816.
(56) Li, J.; Zhong, Q.; Yao, Y.; Bi, S.; Zhou, T.; Guo, X.; Wu, M.; Feng, T.; Xiang, R. Electrochemical performance and thermal stability of the electrospun PTFE nanofiber separator for lithium-ion batteries. *J. Appl. Polym. Sci.* **2018**, *135* (29), 46508.

https://doi.org/10.1021/acsomega.5c03086
ACS Omega 2025, 10, 39669−39679